Astron. Astrophys. 346, 969–978 (1999)

ASTRONOMY AND ASTROPHYSICS

Evidence for an ionization gradient in the local interstellar medium: EUVE observations of white dwarfs

B. Wolff[1], **D. Koester**[1], **and R. Lallement**[2]

[1] Institut für Theoretische Physik und Astrophysik, Universität Kiel, D-24098 Kiel, Germany (koester,wolff@astrophysik.uni-kiel.de)
[2] Service d'Aeronomie du CNRS, B.P. 3, F-91371 Verrieres-le-Buisson, France (Rosine.Lallement@aerov.jussieu.fr)

Received 20 January 1999 / Accepted 9 April 1999

Abstract. We present an enlarged and homogeneous set of interstellar hydrogen and helium column densities obtained through continuum and ionization edges fitting of nearby hot white dwarfs observed with the Extreme Ultraviolet Explorer (EUVE). We compare the HI columns towards the targets and their locations relative to the soft X-ray cavity contours drawn by Snowden et al. (1998). We then use the inferred ionization degrees of hydrogen and helium (available towards 17 objects) as a database for a search of systematic trends in the local interstellar medium. We find that the ionization degree of helium does not show any trend, with a constant value around 40%. At variance with helium, hydrogen ionization varies within the Local Bubble: there is an ionization increase along the general direction of the Canis Major cavity. These results are consistent with hydrogen being ionized by the Canis Major hot stars Adara and Mirzam. However, the co-existence of fully neutral hydrogen and strongly ionized helium along some l-o-s remains to be explained.

Key words: stars: white dwarfs – ISM: abundances – ISM: structure – ultraviolet: ISM

1. Introduction

White dwarfs of spectral type DA provide an excellent opportunity for the study of the hydrogen and helium content of the local interstellar medium revealed by absorption edges from H I (912 Å), He I (504 Å), and He II (228 Å) and the auto-ionization feature from He I (206 Å). Because of their (nearly) pure hydrogen atmospheres, DA white dwarfs emit significant flux at extreme ultraviolet wavelengths, if the effective temperature is greater than ≈ 25000 K. Therefore, these objects are ideal background sources for the detection of interstellar features provided that the atmospheres are not contaminated by traces of heavy elements. This requirement is fulfilled for most DAs with $T_{\rm eff} < 50000$ K as shown by earlier investigations using EUV observations (e.g. Barstow et al. 1997, Wolff et al. 1998).

The local interstellar medium is known to be characterized by the so-called Local Fluff, a group of warm (T = 5,000–10,000 K) clouds within the first 10–20 pc, which are embedded in non-absorbing gas, presumably the hot and tenuous gas which emits the soft X-ray background. The hot gas is supposed to fill the so-called Local Bubble (hereafter LB), a 50–200 pc wide cavity, elongated towards the 3rd quadrant. Recent contours of the LB have been drawn by Welsh et al. (1998), based on sodium absorption, and Snowden et al. (1998), based on the X-ray emission pattern. The origin of the Bubble is not clear yet, and the actual temperature of the hot gas is still a matter of debate (Breitschwerdt & Schmutzler 1994). In addition, there are a number of unanswered questions about the survival of the diffuse clouds inside the bubble, the pressure imbalance between the clouds and the hot gas (Lallement 1998), and the connection of the LB with the neighboring bubbles, as the Loop 1 (Egger & Aschenbach 1995), or the superbubble recently described by Heiles (1998). Details on these questions can be found in Breitschwerdt et al. (1996).

Hydrogen and helium within the warm clouds have been shown to be significantly ionized (Vennes et al. 1993, Dupuis et al. 1995). However, the source of this ionization is still unclear, especially for helium, and the respective roles of the stellar ionizing field, the conductive interfaces between the clouds and the hot gas (Slavin 1998), and previous collisional ionization from a SNR traveling shock (Lyu & Bruhweiler 1996) are still a matter of discussion. The Canis Major stars Mirzam (β CMa) and especially Adara (ε CMa), the strongest EUV source (Vallerga et al. 1993), should be responsible for a significant part of hydrogen ionization (Cheng & Bruhweiler 1990, Vallerga 1996).

2. Observations

The Extreme Ultraviolet Explorer (EUVE) provides the possibility of spectroscopic observations in three spectral bandpasses: 70–190 Å (SW), 140–380 Å (MW), and 280–760 Å (LW). We have used EUVE observations of 29 DA white dwarfs. Most of them were taken from the EUVE archive, supplemented by own observations. The sample comprises all white dwarfs with pure hydrogen atmospheres observed by EUVE and which were accessible to us until December 1998. We have also added some white dwarfs with small contaminations of photospheric heavy elements. These objects are, nevertheless, useful for the determination of interstellar abundances. The full list contains white dwarfs in the temperature range

Send offprint requests to: B. Wolff

Table 1. List of EUVE observations used in this paper. For each star we give the observation dates, the exposure times of the three EUVE spectrometers, and indicate the visibility of the He I (504 Å, 206 Å) and He II (228 Å) features. A "+" denotes the visibility of the feature, a "(+)" means that the feature cannot be distinguished from the noise, and a "−" means that the stellar flux is completely absorbed by the ISM in the spectral range of the feature

WD Number	Name	Observation dates	Exp. times for SW, MW, and LW [ksec]	Visible He features 504 Å	228 Å	206 Å
0004+330	GD 2	1993/10/19–10/20	50.6, 47.5, 48.2	−	−	−
0050−332	GD 659	1994/09/23–09/30	159.6, 149.3, 157.2	−	+	+
0226−615	HD 15638	1993/09/02–09/05	69.0, 69.3, 66.1	−	(+)	(+)
0509−007	RE J0512−00	1997/02/12–02/19	154.4, 152.9, 150.7	−	+	+
0512+326	HD 33959C	1993/01/24–01/26	38.6, 38.6, 39.5	−	(+)	(+)
0549+158	GD 71	1996/12/18–12/22	126.1, 125.3, 122.1	+	(+)	(+)
		1997/02/19–02/21	35.9, 34.7, 35.0			
0630−050	RE J0632−05	1997/10/06–10/09	48.4, 45.7, 46.2	−	−	−
		1997/12/12–12/15	62.5, 58.5, 58.6			
0642−166	Sirius B	1996/11/27–12/07	208.9, 194.7, 200.6	+	(+)	(+)
0715−703	RE J0715−70	1995/09/02–12/02	77.0, 76.2, 71.8	−	−	−
0721−276	RE J0723−27	1996/02/07–02/12	102.3, 97.5, 100.8	+	+	(+)
1029+537	RE J1032+53	1995/04/07–04/15	230.3, 217.3, 220.8	−	+	+
1057+719	PG 1057+719	1994/01/05–01/07	58.5, 57.1, 55.9	−	−	−
		1994/02/21–02/22	57.1, 56.4, 55.1			
1123+189	PG 1123+189	1995/03/13–03/19	201.5, 198.8, 190.8	−	+	+
1234+482	PG 1234+482	1996/03/07–03/10	67.2, 65.8, 65.6	−	+	+
		1996/03/12–03/16	130.4, 130.8, 127.3			
1254+223	GD 153	1993/02/09–02/11	52.0, 54.5, 50.9	+	(+)	(+)
		1993/03/04–03/04	26.5, 26.9, 25.8			
		1993/04/05–04/06	30.2, 29.8, 27.6			
1314+293	HZ 43A	1997/06/25–06/26	28.4, 28.0, 27.7	+	+	(+)
1543−366	RE J1546−36	1998/04/04–04/07	71.5, 67.5, 65.7	−	−	−
		1998/04/11–04/14	68.9, 67.5, 66.9			
1620−391	CD -38°	1993/05/19–07/02	107.2, 103.3, 102.4	−	−	−
1631+781	RE J1629+780	1996/11/04–11/08	106.3, 105.4, 103.8	−	−	−
1658+440	PG 1658+440	1997/06/01–06/08	355.0, 338.2, 366.8	−	(+)	(+)
1740−706	RE J1746−703	1996/03/27–04/05	186.2, 185.4, 186.7	−	−	−
1845+019	Lanning 18	1992/06/28–06/29	27.1, 27.1, 27.1	−	(+)	(+)
		1993/06/22–06/23	35.3, 35.1, 34.0			
2004−605	RE J2009−60	1994/07/09–07/13	106.5, 102.9, 101.8	−	(+)	+
2020−425	MCT 2020−4234	1992/07/18–07/19	34.4, 35.5, 35.6	−	−	−
2124+191	IK Peg	1993/07/23–07/27	92.7, 87.5, 90.0	−	(+)	(+)
2152−548	RE J2156−54	1995/07/24–07/29	149.1, 148.2, 137.2	−	+	+
2247+583	Lanning 23	1997/07/19–07/24	80.4, 72.1, 86.9	−	−	−
		1997/07/29–07/30	16.1, 15.8, 16.9			
2309+105	GD 246	1994/07/16–07/17	35.0, 34.9, 32.2	−	+	+
		1994/08/08–08.08	14.0, 13.2, 13.4			
2321−549	RE J2324−54	1995/07/29–08/05	176.4, 177.3, 164.9	−	+	+

of $T_{\rm eff} \approx 25000$–$59000$ K. Table 1 gives an overview of the observations.

The EUVE spectra were reduced, flux calibrated, and subtracted from contributions of higher orders with the standard procedures of the IRAF/EUV software package. Multiple observations of the same object were co-added according to the exposure times.

Dupuis et al. (1995) have found evidence that the contributions of higher orders to the LW flux are overestimated by the standard calibration. This is taken into account by dividing the LW effective areas of the second, third, and fourth order by their correction factors of 1.4, 1.2, and 1.1, respectively.

The microchannel plate detectors of the EUVE spectrometers are known to add a so-called fixed pattern noise to the spectra. This effect can be reduced by the "dithered" observation mode using randomly chosen pointings near the target. Most observations in our sample have been performed in this operation mode.

We have rebinned each spectrum to a resolution of 1 or 2 Å in order to increase the signal-to-noise ratio and to account for

residual variations due to fixed pattern noise. The flux error for each wavelength interval is the standard deviation of the mean flux ($\sigma_{\rm mean}/\sqrt{n}$). For bright sources like HZ 43A, this error is usual of the order of 5 % and about five times larger than the error of the weighted mean (calculated from the standard deviations of the individual bins). An error of five per cent is expected from the residual fixed pattern noise (e.g. Barstow et al. 1997).

3. Analysis

The first step in analyzing the EUVE spectra and in determining interstellar parameters requires the reproduction of the stellar flux. This is achieved with the use of LTE model atmospheres (see Koester (1996) for a description of the basic methods). For the reproduction of observed EUVE spectra the following parameters need to be determined: solid angle, effective temperature, surface gravity, atmospheric composition, and interstellar column densities of H I, He I, and He II. To facilitate the analysis we fix $T_{\rm eff}$ and $\log g$ at values determined from analyses of hydrogen Balmer lines (mainly taken from Finley et al. 1997). Then, the solid angle can be determined from the predicted flux at 5500 Å and the observed visual magnitude. With the assumption of a pure hydrogen atmosphere – which is valid for most objects in our sample – the remaining parameters are $N(\rm HI)$, $N(\rm HeI)$, and $N(\rm HeII)$.

The interstellar absorption of hydrogen and helium was calculated according to the model of Rumph et al. (1994). The column densities are determined by use of a standard χ^2 technique. However, instead of fitting all three parameters simultaneously, we preferred to fit single features from He I and He II, depending on the visibility of the features. This approach has the advantage that the column densities depend more on the individual features than on the slope of the continuum, which is the case if the full spectral range of EUVE is used all the time.

The visibility of helium features depends strongly on the amount of neutral hydrogen towards the star. An overview can be found in Table 1.

Four objects (HZ 43, GD 71, GD 153, RE J0723−27) of our sample have very low $N(\rm HI)$ values so that the He I absorption edge at 504 Å is visible. In these cases we have first fitted this edge and then varied simultaneously $N(\rm HI)$ and $N(\rm HeII)$. The He II absorption edge can only be seen in two of these objects – in RE J0723−27 and weakly in HZ 43 – so that only these provide a reliable determination of $N(\rm HeII)$.

At somewhat higher hydrogen column densities, several stars show the He II and He I features at 228 Å and 206 Å, respectively, but not the He I absorption edge. In these cases we have fitted the He II edge first and then simultaneously the H I and He I column densities. There are also several stars with such high $N(\rm HI)$ values that no features from helium are visible. Then, we have fixed the He I/H I and He II/H I ratios at mean values (see below) and fitted only the hydrogen column density.

In Tables 2 and 3 we list the results of the analysis together with citations from the literature. The uncertainties of the column densities were determined from the errors in effective temperature and visual magnitude and from the statistical uncertainties of the χ^2 technique. The assumed values for $T_{\rm eff}$ and V are also given in Table 2.

In Table 3 we also list for each object the He I/H I and He II/H I ratios. The weighted means from the objects with detected He I and/or He II features are $\rm He\,I/H\,I = 0.068 \pm 0.002$ and $\rm He\,II/H\,I = 0.052 \pm 0.007$. These errors are included in the determination of $N(\rm HI)$ in those cases where helium features are not visible.

4. Photospheric composition

The photospheric composition is an important parameter for our analysis since it determines the background flux needed for the investigation of interstellar column densities. For all objects with $T_{\rm eff} \leq 50000$ K we have made the assumption of pure hydrogen atmospheres. This is in agreement with previous work showing that most objects in this temperature region can be reasonably well modeled by these atmosphere types (e.g. Barstow et al. 1997, Wolff et al. 1998). During our analysis we could confirm this assumption.

Of special interest are the observations of RE J0632−05, RE J1546−36, and RE J1629+780 since the ROSAT and EUVE photometry of these white dwarfs with effective temperatures below 50000 K indicated the possible presence of additional photospheric absorbers (Jordan et al. 1996, Vennes et al. 1996, Wolff et al. 1996). However, the EUVE spectra do not show any signs of elements beside hydrogen. We could reproduce the spectra using pure hydrogen atmospheres.

We have also analyzed four stars above 50000 K. Three of these objects (GD 246, PG 1123+289, PG1234+482) have already been analyzed by Wolff et al. (1998). For our current analysis we have used their atmospheric compositions of 20% to 40% of the metallicity of G 191-B2B. One object (Lanning 23) has not been analyzed previously. We could infer that this white dwarf does not have a pure hydrogen atmosphere. Its metallicity is approximately 25% and not higher than 50%. Since $N(\rm HI)$ is too high so that helium features are not visible we could determine only an estimate of the hydrogen column density. The error in Table 2 includes the uncertainty of the photospheric composition.

5. H I column density inside the Local Bubble

In Table 4 we summarize the results of the analysis of interstellar column densities and give galactic coordinates and distance estimates for each star.

Distances listed in Table 4 were calculated using the observed visual magnitude and the absolute magnitude as derived from $T_{\rm eff}$, $\log g$, and the evolutionary models of Wood (1992, 1994; "thick layers"). Also given in Table 4 are the distances used for the subsequent search of correlations which are taken from Vennes et al. (1997) for most of them, and from Barstow et al. (1997) for RE J2009−60, and RE J2324−54. For RE J1546−36 and RE J1746−703 the distances used are those

Table 2. Interstellar abundances of neutral hydrogen

WD Number	Name	$T_{\rm eff}$/K	V	$N({\rm HI})/10^{17}\,{\rm cm}^{-2}$	lower limit	upper limit	
0004+330	GD 2	49400 ± 500	13.85 ± 0.01	824.1	756.8	903.6	
0050−332	GD 659	35800 ± 200	13.37 ± 0.02	32.14	24.10	38.19	
				27.0	21.0	33.0	H95
				31.0	23.6	39.1	B97H
				28.7	21.8	35.8	B97S
0226−615	HD 15638	46000 ± 1800		171.8	144.2	223.9	
				120.0	26.0	220.0	B94
0509−007	RE J0512−00	31900 ± 100	13.8 ± 0.3	46.24	29.38	107.4	
0512+326	HD 33959C	40000–47000		73.45	70.96	107.9	
0549+158	GD 71	32700 ± 100	13.032 ± 0.002	6.383	5.728	7.031	
				6.3	4.7	7.9	D95
				6.0	5.3	6.9	B97H
				8.4	7.5	9.5	B97S
0630−050	RE J0632−05	44100 ± 600	15.537 ± 0.015	300.6	265.5	341.2	
0642−166	Sirius B	25100 ± 1000	8.390–8.540	3.4			VM98
				5.248	4.169	6.607	H98
0715−703	RE J0715−70	43900 ± 600	14.178 ± 0.015	217.8	194.5	246.0	
				593.7	98.6	659.2	B97H
				314.3	0.0	693.3	B97S
0721−276	RE J0723−27	35900 ± 200	14.52 ± 0.10	10.00	8.185	11.99	
				9.0			D97
1029+537	RE J1032+53	44000 ± 500	14.455	55.08	41.02	66.68	
				41.6	38.1	46.6	B97H
				39.7	36.8	43.7	B97S
1057+719	PG 1057+719	41500	14.68 ± 0.2	206.5	173.4	391.7	
1123+189	PG 1123+189	54000 ± 2000	14.13 ± 0.03	119.1	96.83	138.4	
				158.0	137.0	180.0	B97H
				102.0	73.0	131.0	B97M
1234+482	PG 1234+482	56000 ± 2000	14.38 ± 0.05	116.7	109.4	163.1	
1254+223	GD 153	38700 ± 200	13.33 ± 0.02	7.907	7.145	8.670	
				9.8	9.0	10.6	D95
				7.8	7.1	8.5	B97H
				7.8	7.1	8.6	B97S
1314+293	HZ 43A	50800 ± 300	12.89	8.851	8.551	9.162	
				8.7	8.1	9.3	D95
				8.8	8.6	9.0	B97H
				8.3	8.2	8.5	B97S
1543−366	RE J1546−36	45200 ± 400	15.81 ± 0.10	503.5	438.5	570.2	
1620−391	CD -38° 10980	25300 ± 100	11.00 ± 0.01	80.17	66.68	95.72	
				167.2	0.0	188.6	B97H
				173.9	0.0	211.7	B97S
1631+781	RE J1629+780	42500 ± 1300	13.04 ± 0.04	278.6	228.0	341.2	
1658+440	PG 1658+440	30500 ± 200	15.02 ± 0.05	28.77	20.37	30.69	
1740−706	RE J1746−703	46400 ± 700	16.60 ± 0.30	173.8	122.2	254.7	
				180.0	140.0	220.0	D&V
1845+019	Lanning 18	29500 ± 300	12.96 ± 0.05	29.51	24.15	34.51	
				19.7	0.0	30.6	B97H
				28.8	0.0	41.2	B97S
2004−605	RE J2009−60	41900 ± 600	13.6 ± 0.3	123.9	83.37	190.5	
				208.6	90.3	314.9	B97H
				162.1	102.8	232.6	B97S
2020−425	MCT 2020−4234	29500 ± 100	14.74 ± 0.30		50.0		
2124+191	IK Peg	34500 ± 100		34.67	29.44	37.33	
				26.9	22.8	34.3	B94
2152−548	RE J2156−54	44300 ± 1100	14.44 ± 0.30	69.66	47.75	92.68	
				58.9	44.8	72.8	B97H
				58.7	57.6	70.3	B97S

Table 2. (continued)

WD Number	Name	$T_{\rm eff}$/K	V	$N({\rm HI})/10^{17}\,{\rm cm}^{-2}$	lower limit	upper limit	
2247+583	Lanning 23	59400	14.26 ± 0.05	779.8	716.1	1596	
2309+105	GD 246	59000 ± 2000	13.09	179.9	153.5	199.5	
				160.0	120.0	160.0	V93
				165.0	144.0	195.0	B97H
				131.0	105.0	137.0	B97M
2321−549	RE J2324−54	41000 ± 1000	15.20	47.42	42.36	77.98	
				43.3	34.0	81.0	B97H
				40.2	35.1	50.5	B97S

V93: Vennes et al. (1993); B94: Barstow et al. (1994); D95: Dupuis et al. (1995); H95: Holberg et al. (1995b)
B97H: Barstow et al. (1997) using homogeneous H+He atmospheres;
B97S: Barstow et al. (1997) using stratified H+He atmospheres;
B97M: Barstow et al. (1997) using atmospheres with metals;
D&V: Dupuis & Vennes (1997); D97: Dupuis et al. (1997); H98: Holberg et al. (1998)
VM98: Vidal-Madjar, priv. comm. (HST GHRS spectrum)

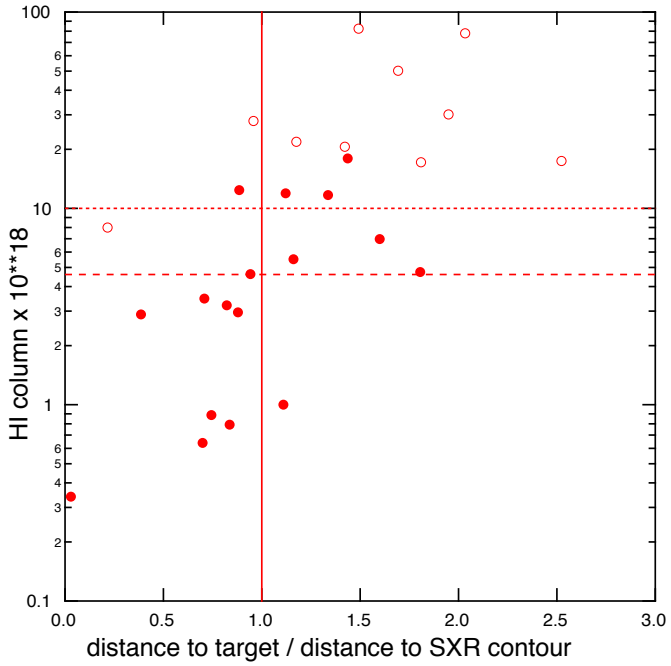

Fig. 1. Location of the stars with respect to the Local Bubble boundary. The neutral hydrogen column density is plotted as a function of the ratio R between the distance to the star and the distance to the Bubble contour in the same direction, estimated from the soft X-ray background (Snowden et al., 1998). If $R < 1$ (> 1), the star is inside (outside) the Bubble. The 17 stars for which helium columns were determined are marked with filled circles

calculated here. In general these two distances are very similar. For the four white dwarfs in close binary systems (HD 15638, HD 33959C, Sirius B, and IK Peg) we have used Hipparcos parallaxes (The Hipparcos and Tycho Catalogues 1997).

In Fig. 1 we have plotted the neutral hydrogen column density as a function of the ratio R between the distance to the star and the distance to the boundary of the Local Bubble estimated from the soft X-ray background emission in the same direction. More precisely, the distance is the one calculated by Snowden et al. (1998) in the frame of the so-called displacement model, for a 1 million K gas in collisional equilibrium in the LB. For each target we have used the contour in the plane closest to the line-of-sight. We estimate the errors on the distances to be of the order of 20 % due to such an interpolation.

The figure can be used to derive a limiting H I column density so that all white dwarfs inside the Local Bubble have a lower column density. Using the distances favored by Snowden et al., this limiting value corresponds to a distance ratio $R = 1$ and is found to be about $N({\rm HI}) = 10^{19}\,{\rm cm}^{-2}$ (dotted line in Fig. 1). However, this value is mainly caused by the unusual high density towards CD -38° 10980. Since circumstellar lines of carbon and silicon are observed in IUE spectra of this star (Holberg et al. 1995a) part of the hydrogen column density may be a result of this circumstellar material. If this object is neglected then the limiting column density can be reduced by a factor of two (dashed line). Apparently, CD -38° 10980 is exceptional in that it has a very large H I column density for a small distance. A second exception is RE J0723−27, which on the contrary has a low column ($1.0 \cdot 10^{18}\,{\rm cm}^{-2}$), but is outside the contours (15–25 % beyond).

The 17 stars for which helium columns were determined are marked with filled circles. It can be seen that for these objects $\log N({\rm HI}) < 19$, and that half of them lie outside the soft X-ray contours represented by Snowden et al. (1998) (i.e. $0 < R < 1.50$–1.75). If the emissivity of the soft X-rays throughout the LB cavity is assumed to be smaller by about 45%, or equivalently the distances to the boundary multiplied by 1.50–1.75, then all these targets would be found to be located within the LB. Such changes are discussed (and not excluded) by Snowden et al. in their interpretation of the X-ray background. This means that we do not know at this stage whether the ionization properties we will discuss in the next section apply to a series of stars all located within the Bubble, or to stars both inside and outside the boundaries. However a better information on the real distances to the LB boundary should be available soon from the combination of precise neutral gas contours (Sfeir et al. 1999) and soft X-ray data.

Table 3. Interstellar abundances of helium

WD Number	Name	$N(\mathrm{HeI})$ $[10^{17}\,\mathrm{cm}^{-2}]$	lower limit	upper limit	$N(\mathrm{HeII})$ $[10^{17}\,\mathrm{cm}^{-2}]$	lower limit	upper limit	HeI/HI	HeII/HI	
0050−332	GD 659	2.624	1.762	3.707	1.618	1.483	1.746	0.082	0.050	
		2.7	2.2	3.2	1.5	1.2	1.8	0.1	0.056	H95
		2.14	1.37	2.86	1.56	1.18	1.90	0.069	0.050	B97H
		2.32	1.64	3.00	1.49	1.18	1.79	0.081	0.052	B97S
0509−007	RE J0512−00	6.427	1.094	10.86	3.614	2.291	4.988	0.139	0.078	
0549+158	GD 71	0.653	0.617	0.692	0.292	0.0	0.573	0.102	0.046	
		0.52	0.44	0.6	0.0	0.0	1.0	0.083	≤ 0.159	D95
		0.45	0.30	0.60	0.02	0.0	0.14	0.075	≤ 0.023	B97H
		1.0	0.82	1.17	0.0	0.0	0.49	0.119	≤ 0.058	B97S
0642−166	Sirius B	0.0	0.0	0.3	0.0	0.0	1.4	≤ 0.09	≤ 0.4	
		0.0	0.0	0.832	0.0	0.0	0.661	≤ 0.158	≤ 0.126	H98
0721−276	RE J0723−27	1.282	1.211	1.358	1.910	1.000	2.844	0.128	0.191	
		1.0			1.6			0.111	0.178	D97
1029+537	RE J1032+53	4.178	2.838	5.781	2.624	2.443	2.805	0.076	0.048	
		5.69	5.19	6.06	2.07	1.50	2.68	0.137	0.050	B97H
		5.76	5.33	6.08	2.73	2.74	3.00	0.145	0.069	B97S
1123+189	PG 1123+189	11.08	9.931	12.47	3.319	3.062	3.614	0.093	0.028	
		9.8	8.1	11.4	3.89	2.79	4.92	0.062	0.025	B97H
		14.3	12.2	16.3	3.64	2.82	4.25	0.140	0.036	B97M
1234+482	PG 1234+482	9.419	6.855	10.59	4.207	4.018	4.436	0.081	0.036	
1254+223	GD 153	0.488	0.462	0.515	0.0	0.0	0.448	0.062	0.0	
		0.66	0.59	0.73	0.0	0.0	1.0	0.067	≤ 0.102	D95
		0.61	0.48	0.72	0.0	0.0	0.27	0.078	≤ 0.035	B97H
		0.66	0.51	0.79	0.0	0.0	0.45	0.085	≤ 0.058	B97S
1314+293	HZ 43A	0.562	0.546	0.573	0.350	0.154	0.527	0.064	0.040	
		0.55	0.52	0.58	0.0	0.0	0.7	0.063	≤ 0.080	D95
		0.65	0.62	0.69	0.44	0.28	0.62	0.074	0.05	B97H
		0.65	0.63	0.68	0.41	0.29	0.54	0.078	0.049	B97S
1658+440	PG 1658+440	0.140	0.0	1.611	2.366	1.589	3.214	0.005	0.082	
1845+019	Lanning 18	2.244	0.914	3.945	0.980	0.345	1.742	0.076	0.033	
		0.0	0.0	2.71	2.38	0.01	3.78	0.0	0.121	B97H
		0.27	0.0	4.00	2.44	0.0	4.04	0.009	0.085	B97S
2004−605	RE J2009−60	11.27	8.974	13.21	6.209	5.333	7.112	0.091	0.050	
		7.99	0.0	14.10	0.35	0.0	10.06	≤ 0.068	≤ 0.048	B97H
		11.97	6.961	16.18	3.27	0.0	5.97	0.074	≤ 0.037	B97S
2124+191	IK Peg	0.838	0.457	1.618	0.643	0.303	1.227	0.024	0.019	
		2.24	1.47	2.69	0.83	0.48	1.21	0.083	0.031	B94
2152−548	RE J2156−54	4.519	1.758	7.278	4.140	3.864	4.436	0.065	0.059	
		5.45	4.07	6.95	3.47	2.71	3.49	0.093	0.059	B97H
		5.34	4.12	6.99	3.65	3.27	4.10	0.091	0.062	B97S
2309+105	GD 246	9.705	8.337	11.64	4.742	4.467	5.047	0.054	0.026	
		10.5			3.7	3.5	4.0	0.065	0.023	V93
		11.0	9.3	12.6	4.41	3.15	5.17	0.067	0.027	B97H
		12.6	10.3	14.5	3.68	2.93	4.41	0.096	0.028	B97M
2321−549	RE J2324−54	7.925	4.446	9.977	4.819	4.121	5.585	0.167	0.100	
		8.84	5.39	10.18	1.29	0.0	2.86	0.204	≤ 0.066	B97H
		9.93	8.98	10.61	9.24	8.40	10.09	0.247	0.230	B97S

6. Ionization of the local interstellar medium

We have used the above set of data in a search for systematic trends in the local interstellar medium properties, and also for relationships between our data and the known interstellar clouds. The former search is made possible by the homogeneity of the set of results, because the same type of modeling has been applied to all spectra.

The most interesting aspect, as we quoted above, is the search for hydrogen and helium ionization gradients, since they are one of the keys for the understanding of the nature and ori-

Table 4. Galactic coordinates, distances, and column densities

WD Number	l^{II}	b^{II}	d/pc[a]	d/pc[b]	$N(\mathrm{HI})/10^{17}\,\mathrm{cm}^{-2}$	HeI/HI	HeII/HI
0004+330	112.48	−28.69	112	97	824.1		
0050−332	299.13	−84.10	70	58	32.1	0.082	0.050
0226−615	284.20	−52.16	199	199	171.8		
0509−007	201.69	−22.29	124	99	46.4	0.139	0.078
0512+326	173.30	−3.35	25	25	73.5		
0549+158	192.03	−5.34	57	49	6.4	0.102	0.046
0630−050	215.38	−6.43	124	156	300.6		
0642−166	227.22	−8.88	2.6	2.6	3.4	≤ 0.090	≤ 0.400
0715−703	281.62	−23.50	82	94	217.8		
0721−276	241.19	−5.93	106	100	10.0	0.128	0.191
1029+537	157.52	+53.24	120	116	55.1	0.076	0.048
1057+719	134.48	+42.92	128	128	206.5		
1123+189	231.90	+68.70	128	112	119.1	0.093	0.028
1234+482	129.81	+69.01	150	129	116.7	0.081	0.036
1254+223	317.25	+84.75	76	67	7.9	0.062	0.0
1314+293	54.10	+84.16	55	67	8.9	0.064	0.040
1543−366	337.83	+13.93	92	92	503.5		
1620−391	341.53	+7.25	14	14	80.2		
1631+781	111.30	+33.58	64	67	278.6		
1658+440	69.12	+38.05	19	27	28.8	0.005	0.082
1740−706	322.77	−20.33	119	119	173.8		
1845+019	34.24	+1.74	43	44	29.5	0.076	0.033
2004−605	336.58	−32.86	53	62	123.9	0.091	0.050
2020−425	358.35	−34.46	72	72	≥ 50.0		
2124+191	70.43	−21.98	46	46	34.7	0.024	0.019
2152−548	339.73	−48.06	120	129	69.7	0.065	0.059
2247+583	107.64	− 0.64	126	122	779.8		
2309+105	87.25	−45.11	76	79	179.9	0.054	0.026
2321−549	326.91	−58.21	155	186	47.4	0.167	0.100

[a] calculated; [b] used for Fig. 1

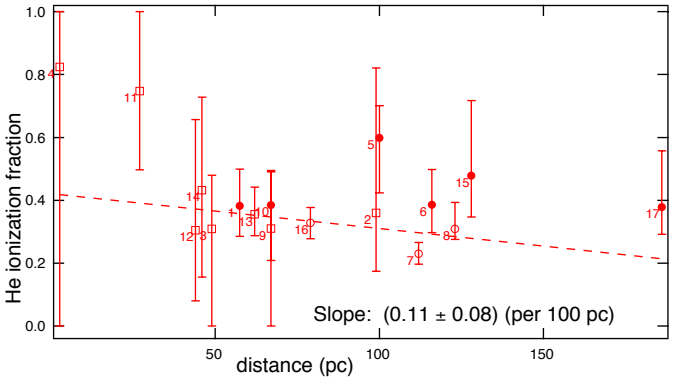

Fig. 2. Ionization fraction of interstellar helium as a function of the distance to the target star. The small gradient found from the linear fit is due to two points with a better precision and is not significant. The error on the slope is of the same order as the slope itself. Filled circles correspond to the "helium-edge" stars. The numbers correspond to the order in Table 3

gin of the Local Bubble. For this search, we have made use of those stars for which helium could be measured (17 objects). For each star, we have assumed that the cosmological abundance ratio of helium to hydrogen is 1:10, and we have derived from the measured column densities of HI, HeI, and HeII the ionization fractions of H and He (see Table 5). The intervals found for the ionization fractions sometimes include negative values, which are of course precluded. However, in order to keep a maximum homogeneity in the analysis, we have considered such values exactly at the same level as the other results, at least for a first analysis. In a second step, we have also compared the resulting trends with those obtained when replacing negative ionization fractions by zero.

We have then searched for eventual correlations between the ionization fractions $f(\mathrm{H}) = \mathrm{H\,II}/(\mathrm{H\,I} + \mathrm{H\,II})$ and $f(\mathrm{He}) = \mathrm{He\,II}/(\mathrm{He\,I} + \mathrm{He\,II})$ and various parameters as the distance, the quantity of gas, and the direction.

For helium, *no* tendency comes out from this search: i.e., it is not possible to get a correlation, at least within the remaining uncertainties. Fig. 2 shows the ionization of helium as a function of the distance, and a linear fit to the data. The error on the slope is of the same order as the slope itself, showing that there is no clear correlation. The first two closest stars only explain the negative best-fit slope, but when using only those stars for

Table 5. Ionization fractions

WD Number	$f_{\rm H}$	$f_{\rm He}$	$f_{\rm H}$ (min)	$f_{\rm H}$ (max)	$f_{\rm He}$ (min)	$f_{\rm He}$ (max)	
0050−332	0.24	0.38	−0.18	0.56	0.32	0.46	
	0.16	0.42	0.0	0.50	0.29	0.58	B97H
	0.25	0.39	0.0	0.55	0.28	0.52	B97S
0509−007	0.54	0.36	−3.47	0.81	0.31	0.95	
0549+158	0.32	0.31	0.07	0.44	0.0	0.45	
	0.0	0.04	0.0	0.28	0.0	0.32	B97H
	0.16	0.0	0.0	0.55	0.0	0.37	B97S
0721−276	0.69	0.60	0.63	0.71	0.45	0.68	
	0.66	0.62					D97
1029+537	0.19	0.39	−0.26	0.52	0.33	0.46	
	0.47	0.27	0.30	0.56	0.20	0.34	B97H
	0.53	0.32	0.44	0.60	0.29	0.36	B97S
1123+189	0.17	0.23	−0.02	0.38	0.20	0.27	
	−0.15	0.29	0.0	0.16	0.20	0.38	B97H
	0.43	0.20	0.13	0.65	0.15	0.26	B97M
1234+482	0.14	0.31	−0.25	0.27	0.30	0.37	
1254+223			−0.55	0.10	0.0	0.46	
	0.0	0.0	0.0	0.28	0.0	0.36	B97H
	0.0	0.0	0.0	0.43	0.0	0.47	B97S
1314+293	0.03	0.38	−0.16	0.13	0.25	0.47	
	0.19	0.40	0.0	0.34	0.29	0.50	B97H
	0.22	0.39	0.08	0.33	0.30	0.47	B97S
1658+440	−0.15	0.94	−0.93	0.58	0.67	1.0	
1845+019	0.09	0.30	−0.92	0.39	0.27	0.31	
	0.l7	1.0	0.0	1.0	0.0	1.0	B97H
	0.0	0.90	0.0	1.0	0.0	1.0	B97S
2004−605	0.29	0.36	0.06	0.42	0.35	0.37	
	0.0	0.04	0.0	0.63	0.0	1.0	B97H
	0.0	0.22	0.0	0.54	0.0	0.46	B97S
2124+191	−1.34	0.43	−3.91	−0.03	0.40	0.44	
	0.12	0.27	−0.17	0.12	0.25	0.31	B94
2152−548	0.20	0.48	−0.65	0.59	0.38	0.69	
	0.34	0.39	0.0	0.57	0.28	0.46	B97H
	0.35	0.41	0.05	0.48	0.32	0.50	B97S
2309+105	−0.25	0.33	−0.49	0.05	0.28	0.38	
	−0.14	0.26	−0.15	0.17	0.20	0.34	V93
	−0.06	0.29	0.0	0.19	0.20	0.36	B97H
	0.19	0.23	0.04	0.45	0.17	0.30	B97M
2321−549	0.63	0.38	0.09	0.73	0.36	0.48	
	0.57	0.13	0.0	0.74	0.0	0.35	B97H
	0.79	0.48	0.71	0.83	0.44	0.53	B97S

which HeII and HeI were determined from the helium edges (large dots), the slope disappears. This implies that helium is apparently equally ionized in the solar vicinity, the ionization fraction being found to be around 40%. This is an important aspect, showing that there is no ionizing agent in a particular location. These results confirm, with a larger number of targets and a larger sampled volume, that helium is everywhere significantly ionized (Dupuis et al. 1995).

For hydrogen, the situation is very different. We find a positive correlation between the ionization and the distance of the target (not shown here). But, more important, we find a better correlation with the abscissa of the target along an axis angularly close to the $(l, b) = (228°, -22°)$ direction. This direction coincides with the general direction of the CMa tunnel ($(l, b) = (240°, -11°)$ for ε CMa, and $(l, b) = (226°, -14°)$ for β CMa). Fig. 3 shows the derived hydrogen ionization fraction, plotted as a function of $l = d\cos\varphi$, where d is the distance to the target and φ is the angle between the target and $(l, b) = (228°, -22°)$.

The ionization of hydrogen is shown to increase when the l-o-s is closer to the CMa wake. The strength of the correlation can be evaluated from the 1σ error on the slope of the linear fit $df_{\rm H}/dl = 5.6 \pm 1.8 \cdot 10^{-3}\,{\rm pc}^{-1}$. The direction $(l, b) = (228°, -22°)$ corresponds to the maximum ratio between the slope found and the uncertainty on this slope. Replacing negative mean ionization degrees by zero results in a

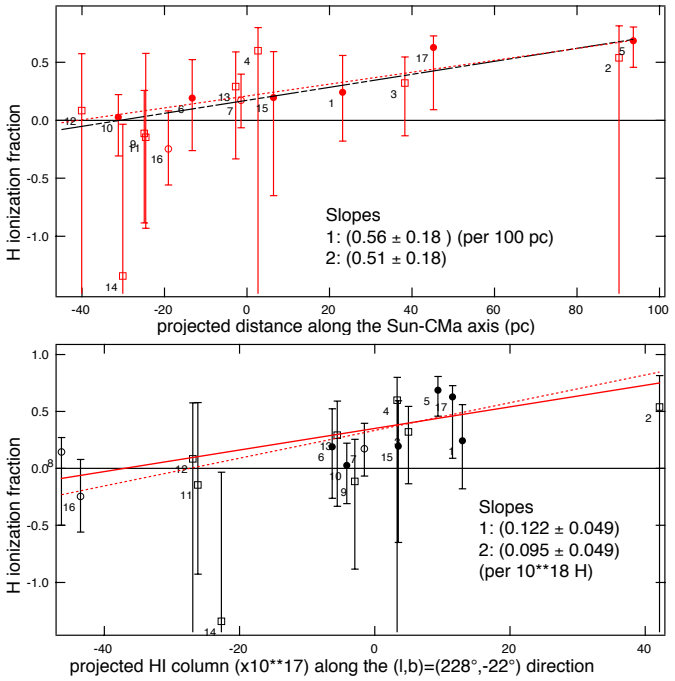

Fig. 3. *Top:* Hydrogen ionization fraction as a function of the projected distance along the $(l, b) = (228°, -22°)$ axis. Filled circles correspond to the "helium-edge" stars. Distances are positive towards this direction. Hydrogen ionization increases along this axis. The first linear fit (dashed line) is obtained using the mean ionization deduced from the spectral analysis, even if the resulting mean ionization fraction is negative (see text). The second fit is obtained by replacing negative mean ionization by zero. The quoted (standard deviation) error on the slope is calculated using for each data point half the total interval allowed as the 1σ error. *Bottom:* Hydrogen ionization fraction as a function of the projected HI column density along the $(l, b) = (228°, -22°)$ axis. The average ionization degree gradient is of the order of $12 \cdot 10^{-3}$ per 10^{17} atoms column (i.e. a variation from $f_{\rm H} = 0$ (neutral gas) to $f_{\rm H} = 1$ (fully ionized gas) for a column $N(HI) = 8 \cdot 10^{18}\,{\rm atoms\,cm^{-2}}$)

slight decrease of the slope $df_{\rm H}/dl = 5.1 \pm 1.8 \cdot 10^{-3}\,{\rm pc}^{-1}$. If we keep only the "helium-edge" stars (large dots), the slope and the error remain of the same order. We then conclude that there is evidence for an ionization gradient of H along the CMa direction. Further measurements should help to establish it more firmly, especially with more stars in directions close to the CMa direction, like GD71.

Now, reconsidering the correlation with distance quoted above, it appears as a secondary effect, due to the fact that there are more distant targets towards the CMa wake compared with other regions with a closer boundary. Indeed, there is a correlation between the distance to the target and the angle φ (not shown here). We thus conclude that the primary effect is likely the ionization gradient along the CMa-Sun axis, and the correlation between the ionization and the distance is an observational bias. Fig. 3 shows also the ionization degree of H as a function of the projected HI column density, i.e. the product of the l-o-s total column by cos(φ). If the gas was homogeneously distributed, this projected column would represent, within an additional constant, the column of gas encountered by photons from the CMa hot stars. This allows to get an idea of the spatial gradient of the ionization degree, here of the order of $12 \cdot 10^{-2}$ per 10^{18} cm^{-2} column, i.e. about 5 times weaker than what ionization models predict (Vallerga 1996). However, the medium is inhomogeneous and the line-of-sight may cross different cloudlets. In this case the gradient we have derived here cannot be directly compared with a model assuming a simple homogeneous slab of gas, and a better modeling is required.

7. Conclusion and discussion

EUVE spectra of hot white dwarfs, when analyzed in a homogeneous way, show evidence for a gradient of the interstellar hydrogen ionization along an axis oriented along the Sun-Canis Major direction. This is the first observational evidence for the gradient predicted by Vallerga (1996) and this opens new perspectives on the role of the CMa B stars and the CMa cavity, and on the relative influence of ionization by hot stars and by background emission.

At variance with hydrogen, helium ionization does not show any strong trend, in agreement with predictions of the photo-ionization models (Cheng & Bruhweiler 1990, Vallerga 1996). However, photo-ionization alone cannot explain the large ionization degree of helium. Helium ionization is then probably linked to a non equilibrium state, as suggested by Lyu & Bruhweiler (1996). According to their model, if a SNR expanding shock has totally ionized the local ISM and recombination is not achieved, hydrogen and helium ionization degrees of the order of 40% could be reached after about a million years. Both phenomena, i.e. fossile ionization after a SNR shock and photo-ionization by hot stars can be made compatible with the observed ionization properties, at least when hydrogen and helium are both significantly ionized. Still, since both H and He recombine with about the same timescale, it remains to explain how hydrogen can be fully neutral and helium simultaneously 30–40% ionized, as it is found along some of the line-of-sights. More data are certainly needed to investigate further the characteristics of different types of ISM. However, the present study illustrates how EUV spectra of white dwarfs can shed new light on the physical processes in the local interstellar medium.

Acknowledgements. This work has been supported by the Deutsches Zentrum für Luft- und Raumfahrt (DLR) under grant 50 OR 96173. We have made use of the Simbad data base, operated at CDS, Strasbourg, France.

References

Barstow M.A., Holberg J.B., Koester D., 1994, MNRAS 270, 516
Barstow M.A., Dobbie P.D., Holberg J.B., Hubeny I., Lanz T., 1997, MNRAS 286, 58
Breitschwerdt D., Schmutzler T., 1994, Nat 371, 774
Breitschwerdt D., Freyberg M.J., Trümper J. (eds.), 1996, The Local Bubble and Beyond. Lecture Notes in Physics, Springer, Berlin
Cheng K.P, Bruhweiler F.C., 1990, ApJ 364, 573
Dupuis J., Vennes S., 1997, ApJ 475, L131
Dupuis J., Vennes S., Bowyer S., Pradhan A., Thejll P., 1995, ApJ 455, 574

Dupuis J., Vennes S., Bowyer S., 1997, In: Isern J., Hernanz M., Garcia-Berro E. (eds.), White Dwarfs. Kluwer, Dordrecht, p. 277
Egger R., Aschenbach B., 1995, A&A 294, L25
Finley D.S., Koester D., Basri G., 1997, ApJ 488, 375
Heiles C., 1998, ApJ 498, 689
Holberg J.B., Bruhweiler F.C., Andersen J., 1995a, ApJ 443, 753
Holberg J.B., Barstow M.A., Bruhweiler F.C., Sion E.M., 1995b, ApJ 453, 313
Holberg J.B., Barstow M.A., Bruhweiler F.C., Cruise A.M., Penny A.J., 1998, ApJ 497, 935
Jordan S., Finley D., Koester D., Wolff B., 1996, In: Zimmermann H.U., Trümper J.E., Yorke H. (eds.) Röntgenstrahlung from the Universe. MPE Report 263, Garching, p. 5
Koester D., 1996, In: Bowyer S., Malina R.F. (eds.), Astrophysics in the Extreme Ultraviolet. Kluwer, Dordrecht, p. 185
Lallement R.., 1998, In: Breitschwerdt, et al. (eds.) The Local Bubble and Beyond. Lecture Notes in Physics, Springer, Berlin, p. 19
Lyu C., Bruhweiler F., 1996, ApJ 459, 216
Rumph T., Bowyer S., Vennes S., 1994, AJ 107, 2108
Sfeir, D., Lallement R., Crifo F., Welsh B.Y., 1999, A&A, submitted
Slavin J., 1998, In: Breitschwerdt, et al. (eds.) The Local Bubble and Beyond. Lecture Notes in Physics, Springer, Berlin, p. 169
Snowden S.L., Egger R., Finkbeiner D.P., Freyberg M.J., Plucinsky P.P., 1998, ApJ 493, 715
The Hipparcos and Tycho Catalogues, 1997, Vol. 1–16, ESA Publications Division, Noordwijk
Vallerga J., 1996, Space Sci. Rev., 78, 277
Vallerga J., Vedder P., Welsh B.Y., 1993, ApJ 414, L65
Vennes S., Dupuis J., Rumph T., et al., 1993, ApJ 410, L119
Vennes S., Thejll P.A., Wickramasinghe D.T., Bessell M.S., 1996, ApJ 467, 782
Vennes S., Thejll P.A., Genova Galvan R., Dupuis J., 1997, ApJ 480, 714
Welsh B.Y., Crifo F., Lallement R., 1998, A&A 333, 101
Wolff B., Jordan S., Koester D., 1996, A&A 307, 149
Wolff B., Koester D., Dreizler S., Haas S., 1998, A&A 329, 1045
Wood M.A., 1992, ApJ 386, 539
Wood M.A., 1994, In: Chabrier G., Schatzman E. (eds.) The Equation of State in Astrophysics, IAU Coll. 147, Cambridge University Press, p. 612